Received: 10 March 2023 | Revised: 22 June 2023 | Accepted: 3 July 2023

DOI: 10.1002/mrm.29802

RESEARCH ARTICLE

Magnetic Resonance in Medicine

Motion-resolved four-dimensional abdominal diffusion-weighted imaging using PROPELLER EPI (4D-DW-PROPELLER-EPI)

Lu Wang[1,2] | **Tian Li**[1] | **Jing Cai**[1] | **Hing-Chiu Chang**[3,4]

[1]Department of Health Technology and Informatics, The Hong Kong Polytechnic University, Hong Kong, Hong Kong

[2]Department of Diagnostic Radiology, Li Ka Shing Faculty of Medicine, The University of Hong Kong, Hong Kong, Hong Kong

[3]Department of Biomedical Engineering, The Chinese University of Hong Kong, Hong Kong, Hong Kong

[4]Multi-Scale Medical Robotics Center, The Chinese University of Hong Kong, Hong Kong, Hong Kong

Correspondence
Hing-Chiu Chang, Department of Biomedical Engineering, The Chinese University of Hong Kong, Room 1112, 11/F, William M.W. Mong Engineering Building, Shatin, N.T., Hong Kong.
Email: hcchang@cuhk.edu.hk

Funding information
Hong Kong Research Grant Council, Grant/Award Numbers: ECS 24213522, GRF 17106820, GRF 17125321

Abstract

Purpose: To develop a distortion-free motion-resolved four-dimensional diffusion-weighted PROPELLER EPI (4D-DW-PROPELLER-EPI) technique for benefiting clinical abdominal radiotherapy (RT).

Methods: An improved abdominal 4D-DWI technique based on 2D diffusion-weighted PROPELLER-EPI (2D-DW-PROPELLER-EPI), termed 4D-DW-PROPELLER-EPI, was proposed to improve the frame rate of repeated data acquisition and produce distortion-free 4D-DWI images. Since the radial or PROPELLER sampling with golden-angle rotation can achieve an efficient k-space coverage with a flexible time-resolved acquisition, the golden-angle multi-blade acquisition was used in the proposed 4D-DW-PROPELLER-EPI to improve the performance of data sorting. A new k-space and blade (*K*-B) amplitude binning method was developed for the proposed 4D-DW-PROPELLER-EPI to optimize the number of blades and the k-space uniformity before performing conventional PROPELLER-EPI reconstruction, by using two metrics to evaluate the adequacy of the acquired data. The proposed 4D-DW-PROPELLER-EPI was preliminarily evaluated in both simulation experiments and in vivo experiments with varying frame rates and different numbers of repeated acquisition.

Results: The feasibility of achieving distortion-free 4D-DWI images by using the proposed 4D-DW-PROPELLER-EPI technique was demonstrated in both digital phantom and healthy subjects. Evaluation of the 4D completeness metrics shows that the *K*-B amplitude binning method could simultaneously improve the acquisition efficiency and data reconstruction performance for 4D-DW-PROPELLER-EPI.

Conclusion: 4D-DW-PROPELLER-EPI with *K*-B amplitude binning is an advanced technique that can provide distortion-free 4D-DWI images for resolving respiratory motion, and may benefit the application of image-guided abdominal RT.

KEYWORDS

4D-DWI, distortion-free images, golden angle, *K*-B amplitude binning, PROPELLER-EPI

1 | INTRODUCTION

4D-CT has been widely used in abdominal image-guided radiotherapy (IGRT)[1] for improving the precision and accuracy of the treatment procedure, despite its extra radiation exposure and poor contrast in soft tissue.[2] Recently, 4D-MRI has become an emerging technique in abdominal IGRT that can overcome the drawbacks of 4D-CT because of its non-invasive property, high contrast in soft tissue, and flexibility in imaging orientation.[3] 4D-MRI techniques can be typically categorized into prospective 4D-MRI and retrospective 4D-MRI, of which the former acquires data at preset motion directly, whereas the latter acquires data at various motions and then sorts them.[3] In addition, the sorting of data for resolving the abdominal motion using either amplitude or phase binning method is usually based on a surrogate respiratory signal concurrently recorded during data acquisition. With these developments, the mainstream 4D-MRI techniques have successfully achieved different conventional image contrasts, such as T_1-, T_2-, and T_1/T_2-weighted imaging.[4]

Although the mainstream 4D-MRI techniques can provide various image contrasts with complementary information, the tumor-to-tissue contrast may still be insufficient for abdominal IGRT applications, especially without the administration of MRI contrast agents. In addition to conventional image contrast, DWI can provide both structural and functional information with improved tumor-to-tissue contrast, and has been integrated into the routine practice of abdominal MRI.[5,6]

To date, the feasibility of the motion-resolved 4D-DWI technique has been demonstrated by using routine diffusion-weighted single-shot EPI (DW-ss-EPI), referred to as 4D-DW-ss-EPI.[7] It synchronously acquired repeated abdominal DWI images and surrogate respiratory signals over multiple respiratory cycles and then sorted image data into several phase bins according to the corresponding respiratory waveform. The sorted images with different diffusion encoding directions of each bin were averaged for producing the final 4D-DWI dataset. This important study first shows that the abdominal 4D-DWI may provide superior tumor-to-tissue contrast to conventional 4D-MRI and also be capable of simultaneously measuring the functionality of tissue.

However, the performance of 4D-DW-ss-EPI is currently limited because the abdominal DWI is particularly challenging when using DW-ss-EPI. First, the geometric distortions and blurring artifacts caused by more prominent field inhomogeneity and T_2^* decay can lead to low image quality and insufficient geometric accuracy in abdominal DW-ss-EPI.[8–10] In addition, cardiac motion, respiration, and voluntary movements can further degrade the image quality and increase the challenge in achieving robust abdominal DW-ss-EPI.[6,11–13] Moreover, significant variations in amplitude and period of surrogate respiratory signal and the relatively low frame rate of repeated image acquisition can aggravate the image blurring in 4D-DW-ss-EPI after data binning.[7,14]

Several developed techniques may potentially alleviate the challenges of abdominal 4D-DW-ss-EPI. Parallel imaging techniques, such as SENSE[15] and GRAPPA,[16] have been used to reduce the geometric distortions and image blurring for abdominal DW-ss-EPI,[17,18] at the cost of undesired noise amplification when using high acceleration factors. In addition, multi-shot EPI techniques (ms-EPI), such as interleaved EPI (iEPI) with multiplexed sensitivity encoding (MUSE),[19,20] and readout-segmented EPI (rs-EPI),[21,22] can significantly improve the image quality of brain and abdominal DWI,[23,24] but often require additional navigator echo or advanced calculation for removing the data inconsistency due to shot-to-shot phase variations. A self-navigated ms-EPI technique, namely PROPELLER-EPI, can perform robust phase correction and has been proposed to achieve high-resolution DWI,[25] Q-ball imaging,[26] SWI,[27] fMRI,[28] and echo planner time-resolved imaging (EPTI)[29] for different brain applications with improved geometric fidelity, reduced susceptibility to subject motion, and better acquisition efficiency enabled by the data sharing among the blades. In addition, a preliminary study also demonstrated the high-quality and robust liver DWI being achieved by using PROPELLER-EPI[30,31] under free-breathing conditions.

In this study, we proposed an improved abdominal 4D-DWI technique based on 2D diffusion-weighted PROPELLER-EPI (2D-DW-PROPELLER-EPI), termed 4D-DW-PROPELLER-EPI, to improve the frame rate of repeated data acquisition and produce distortion-free motion-resolved 4D-DWI images. Since the radial or PROPELLER sampling with golden-angle rotation can achieve an efficient k-space coverage with a flexible time-resolved acquisiton,[32–35] the golden-angle multi-blade acquisition was also used in the proposed 4D-DW-PROPELLER-EPI to improve the performance of data sorting. In addition, a new k-space and blade (*K*-B) amplitude binning method was developed for the proposed 4D-DW-PROPELLER-EPI to optimize the number of blades and the uniformity of k-space before performing conventional PROPELLER-EPI reconstruction, by using two metrics to evaluate the adequacy of the acquired data. The proposed 4D-DW-PROPELLER-EPI was preliminarily evaluated in both simulation experiments and in vivo experiments with varying frame rates and different numbers of repeated acquisitions.

2 | METHODS

2.1 | Flowchart of 4D-DW-PROPELLER-EPI

Figure 1A shows the overall flowchart of the proposed motion-resolved abdominal 4D-DW-PROPELLER-EPI, which mainly consists of 2D-PROPELLER-EPI imaging, retrospective data binning, and conventional PROPELLER-EPI reconstruction. After the repeated acquisition of DWI data using PROPELLER-EPI sampling, Nyquist ghost correction was performed for each blade. Then, for the data of each diffusion direction, the *K*-B amplitude binning method was used to sort the blades into several bins according to the corresponding respiratory cycle during data acquisition. Next, the sorted blade data for each bin along each diffusion direction were reconstructed with the conventional PROPELLER-EPI reconstruction method. Finally, the reconstructed 4D-DWI datasets for the three orthogonal diffusion directions were combined to produce the final abdominal 4D-DWI images by taking the geometric mean. The details of each acquisition or processing step are described in the subsections below.

2.2 | Data acquisition

The acquisition of the originally proposed 4D-DW-ss-EPI technique based on conventional 2D DW-ss-EPI includes[7] (Figure 1B, left): (1) one image dataset acquired with T_2-weighted ss-EPI (T_{2W}-ss-EPI at b-value = 0 s/mm^2) and three individual image datasets acquired with DW-ss-EPI along x, y, and z diffusion directions under free-breathing; and (2) the surrogate respiratory signals synchronously recorded during the image acquisition. The full coverage of the whole liver required a TR of 6000 ms. In order to improve the frame rate and geometric fidelity, the 2D-DW-PROPELLER-EPI pulse sequence was used to sample the 4D-DWI datasets with long-axis multi-blades (Figure 1B, right) instead of conventional 2D DW-ss-EPI.

The rotation angle and the number of blades are two crucial parameters in 2D-DW-PROPELLER-EPI acquisition, and often the fixed values (i.e., linear-angle rotation)

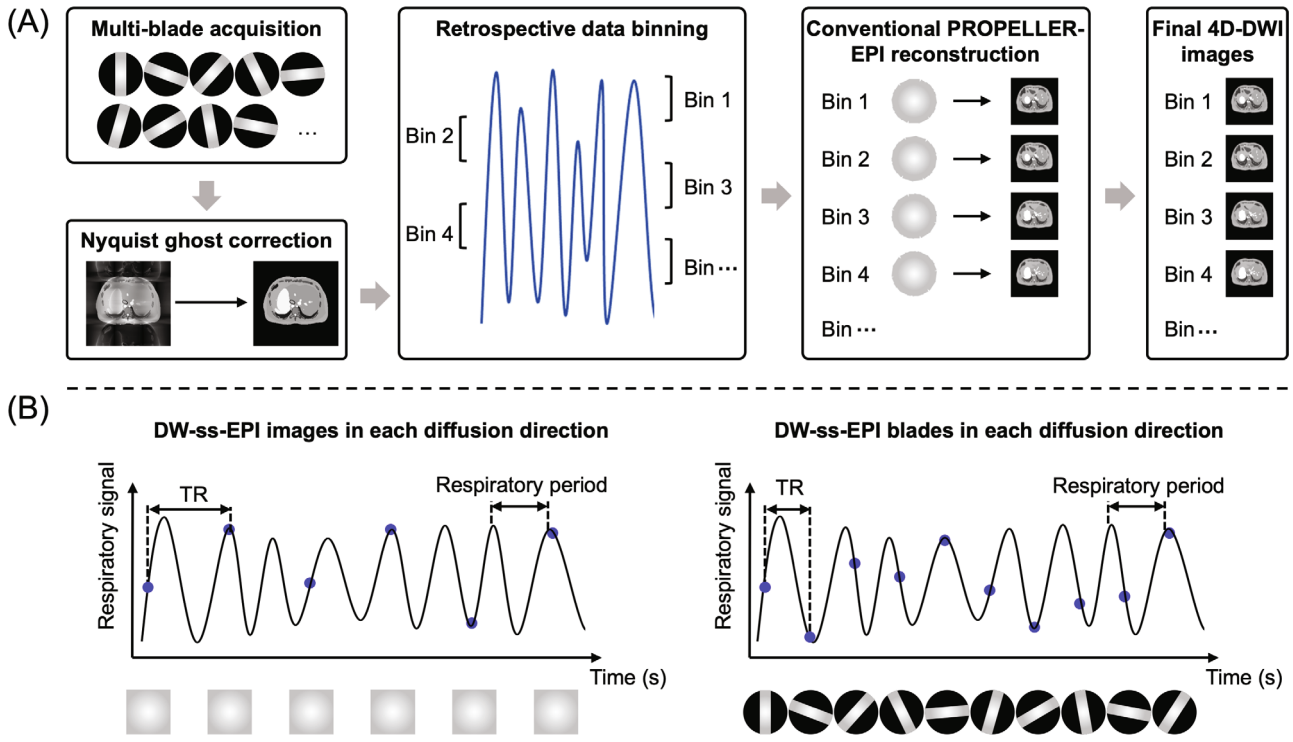

FIGURE 1 (A) Overview of the flowchart of the proposed motion-resolved abdominal 4D-DW-PROPELLER-EPI with the schematic illustration of the acquisition in one diffusion direction. Nyquist ghost correction was firstly performed for each blade after the multi-blade acquisition with golden-angle rotation. Then, for each diffusion direction, all blades were binned retrospectively using the *K*-B amplitude binning method. Afterward, images were reconstructed by the conventional PROPELLER-EPI reconstruction for each diffusion direction. Finally, 4D-DWI images were produced by combining 4D-DWI datasets produced from the three orthogonal diffusion directions. (B) Data acquisition of the originally proposed 4D-DW-ss-EPI technique (left) and proposed 4D-DW-PROPELLER-EPI technique (right). Full k-space data were acquired for the former while rotated blades were acquired for the latter.

which are determined by the blade size (i.e., frequency and phase encoding matrix for each blade), target resolution, and the effective number of excitation (NEX).[33,36] Whereas for 4D-DW-PROPELLER-EPI, the linear-angle rotation of blades for sampling the k-space with multiple 360° circular coverages may be suboptimal to form a sufficient sampling of k-space after binning the over-sampled blades. In other words, the coherency between the repeated acquisition of blades and respiratory cycles may occur, possibly leading to the redundancy of blades or the insufficiency of k-space data for a single bin. To address this problem, the golden-angle[32–35] multi-blade acquisition (i.e., rotation angle = 111.25°) was used for introducing improved temporal incoherency between the sampling of blades and respiratory cycles.

In motion-resolved 4D-DWI, the other two important parameters are the number of repeated acquisitions (N_r) and frame rate (F_s) of repeated acquisitions for each slice location. N_r is defined as the total number of multi-blades for 4D-DW-PROPELLER-EPI. F_s is equivalent to the inverse of TR (1/TR) for both 4D-DW-ss-EPI and 4D-DW-PROPELLER-EPI. However, the attainable frame rate (i.e., inversely proportional to the shortest TR) for 4D-DW-ss-EPI was limited by the desired slice coverage and image quality (e.g., insufficient SNR due to shortened TR). By using 2D-DW-PROPELLER-EPI, the shortened echo-train length (ETL) of each blade acquisition could improve the frame rate by 50% compared with using ss-EPI for the same slice coverage in our study (i.e., TR of 3000 ms vs. 6000 ms).

2.3 | Nyquist ghost correction

Because of the use of oblique gradient waveforms for multi-blade acquisition in 2D-DW-PROPELLER-EPI, each blade often requires 2D Nyquist ghost correction for better suppression of ghosting artifact.[37] To eliminate the need for additional reference scan and the possible inconsistency between reference and imaging data, the reference-free 2D phase cycled reconstruction (PCR) was adopted to perform the 2D Nyquist ghost correction for each blade before data binning,[38,39] consisting of an iterative column-based reconstruction procedure as follows: (1) the odd and even k-lines of each blade were separated into two undersampled k-spaces and then reconstrutcted to two induvidal images; (2) a single column along phase-encoding direction located at FOV center was selected; (3) 2D PCR generated a set of ghost corrected 1D profiles by cycling through various potential 2D phase errors, and the ghost corrected 1D profile with the lowest artifact level was selected by evaluating the background energy; and (4) the columns adjacent to the previously processed column were selected for performing 2D PCR with the reduced phase cycling range according to the phase errors derived in step 3. The above procedure was repeated until all columns were processed for each blade.

2.4 | *K*-B amplitude binning method and conventional PROPELLER-EPI reconstruction

For 4D-DW-PROPELLER-EPI, the simple use of amplitude or phase binning for sorting all acquired blades into several bins could possibly lead to k-space sampling non-uniformity, resulting in degraded image quality after performing conventional PROPELLER-EPI reconstruction. As shown in Figure 2, the 2D point-spread function (PSF) of PROPELLER-EPI associated with T_2^* decay windowing of blades was prominently affected by the number of blades (N_B) and the k-space sampling uniformity (K_{unif}).

Therefore, to provide the indexes for optimizing data binning, the K_{unif} and N_B were used to evaluate the data sufficiency for PROPELLER-EPI reconstruction after data binning. The K_{unif} for the data sampled with the matrix size of M-by-N was defined as

$$K_{unif} = \frac{1}{MN}\sum_{m=0}^{M-1}\sum_{n=0}^{N-1}\frac{\left|N_{re-grid}(m,n) - N_{des}(m,n)\right|}{N_{des}(m,n)}$$

where $N_{re\text{-}grid}$ represents the number of k-space data points after re-gridding of all collected blades, and N_{des} represents the number of desired k-space data points for PROPELLER-EPI reconstruction. For a given blade size with desired N_B for 360° circular k-space coverage, higher K_{unif} suggests better image quality after PROPELLER-EPI reconstruction of the binned blades (max $K_{unif} = 1.0$).

In 4D-MRI, the completeness of the 4D dataset is evaluated with a 4D completeness metric (Cp), which was defined as the ratio of the number of image-filled bins for all slices ($N_{i,all}$) to the total number of desired bins for all slices ($N_{bin,all}$):

$$Cp(\%) = \frac{N_{i,all}}{N_{bin,all}}$$

To ensure sufficient data for the accurate reconstruction of 4D-MRI, Cp is expected to be equal to or greater than 95%.[40] In the proposed 4D-DW-PROPELLER-EPI, achieving sufficient quality for the reconstructed image relies on both desired N_B and K_{unif}. Therefore, the metrics of 4D completeness of desired N_B (Cpb) and K_{unif} (Cpk) were defined to evaluate the data adequacy for 4D-DW-PROPELLER-EPI:

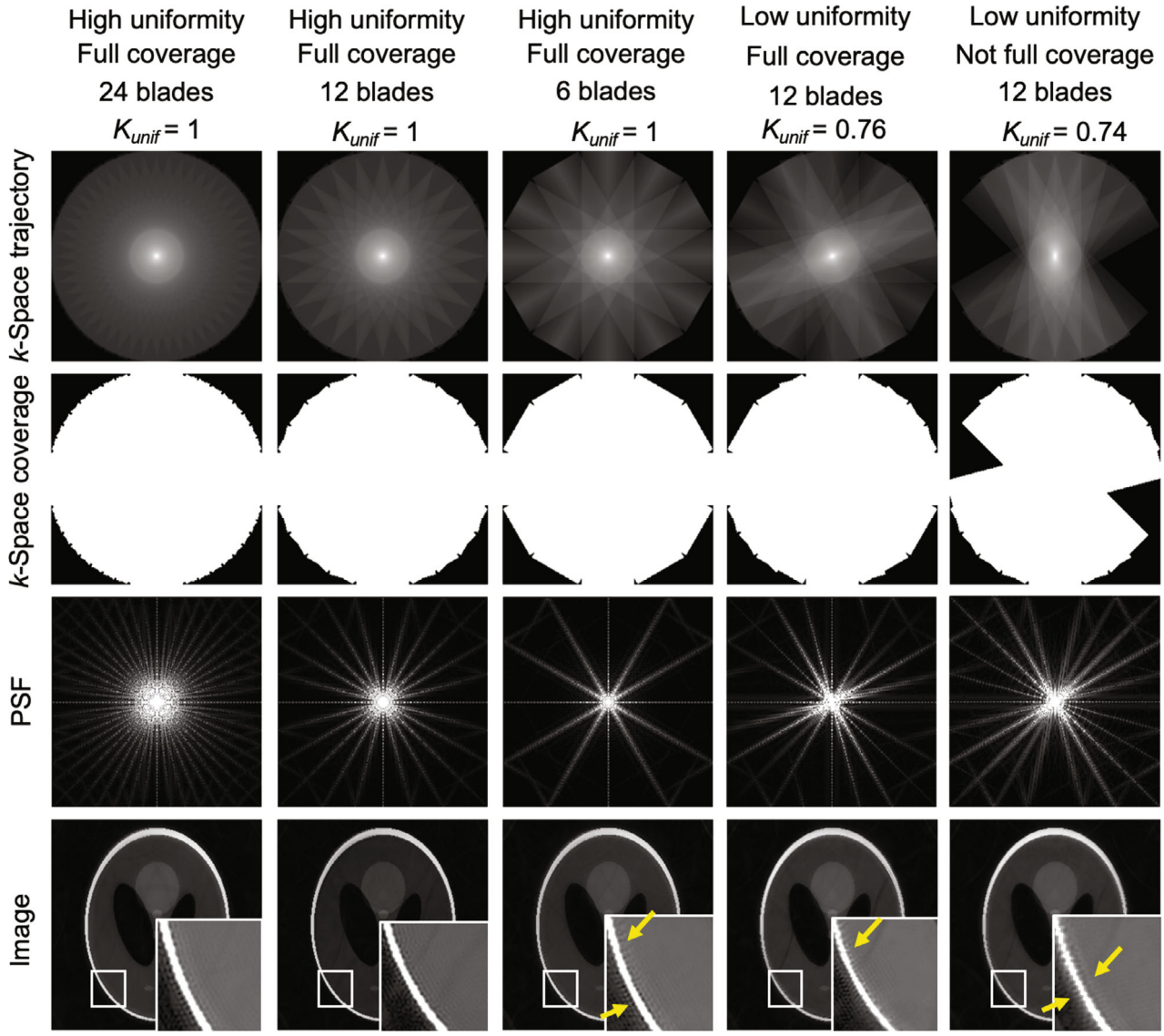

FIGURE 2 Simulated 2D-PROPELLER-EPI acquisitions using the Shepp-Logan digital phantom with different k-space trajectories, and their corresponding k-space coverages, 2D PSFs, and reconstructed images (matrix size = 256 × 256). (A) to (C) Data acquired with high k-space uniformity and full 180° k-space coverage with 24, 12, and 6 blades (blade size = 256 × 64), respectively. (D) Data acquired with low k-space uniformity, and full 180° k-space coverage with 12 blades. (E) Data acquired with low k-space uniformity, and insufficient k-space coverage with 12 blades. Artifacts are pointed by the yellow arrows in the reconstructed images with either low k-space uniformity or insufficient k-space coverage. (A)–(C) A sufficient number of blades (e.g., $N_B \geq 12$) are important for achieving high image quality for 2D-PROPELLER-EPI even if the acquired blades are uniformly distributed in k-space. (B), (D), (E) Uniformity of k-space sampling is also important when blade numbers are sufficient for 180° k-space coverage. In short, both sufficient blades and high k-space uniformity are highly desired for 2D-PROPELLER-EPI.

$$Cpb(\%) = \frac{N_{bin,all>des\_b}}{N_{bin,all}}\#$$

and

$$Cpk(\%) = \frac{N_{bin,all>des\_k}}{N_{bin,all}}\#$$

where $N_{\text{bin,all}>des\_b}$ is the number of bins filled with the blades more than the desired N_B (*des_b*) for all slices, and $N_{\text{bin,all}>des\_k}$ is the number of bins filled with blades that can reach the desired K_{unif} (*des_k*) for all slices.

To simultaneously maximize the K_{unif} and N_B, the *K*-B amplitude binning method was introduced to sort all the blades acquired with golden-angle rotation under free-breathing (Figure 3). First, the interval of each amplitude bin was extended (e.g., producing 10%–20% overlapping between two adjacent bins) to sort all the blades into different bins (Figure 3A). In addition, a single blade could

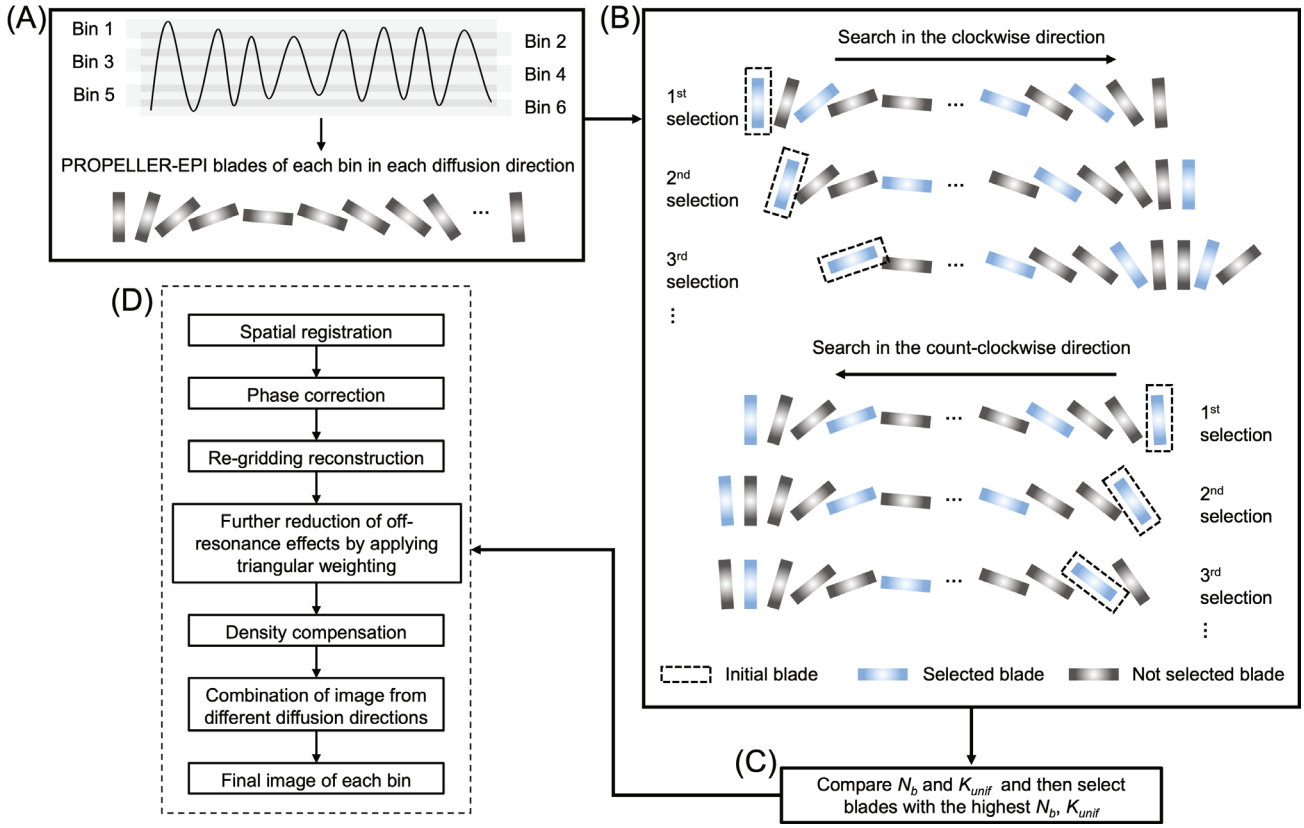

FIGURE 3 Flowchart of *K*-B amplitude binning and the conventional PROPELLER-EPI reconstruction for the proposed 4D-DW-PROPELLER-EPI technique. (A) All blades acquired with golden-angle rotation and same diffusion direction were sorted into different bins according to the extended interval of each amplitude bin. (B) For each slice location, an initial blade was selected from the binned data to start the search of the adjacent blade either in the clockwise or count-clockwise direction until reaching the target N_B for a 180° circular k-space coverage or no available blades fulfilling the predefined angular difference between any pair of two adjacent blades (i.e., +/−10% of desired rotation angle). For the rest of the blades without being selected, one of them was selected as an initial blade for starting another search cycle again with the use of all blades in the same bin. The blade selection process was repeated until all blades in the same bin were selected for at least one combination. (C) The combination of blades with the highest N_B and K_{unif} was selected to produce the image for the corresponding bin by using conventional PROPELLER-EPI reconstruction. (D) A series of conventional PROPELLER-EPI reconstruction steps were performed to produce the final 4D-DWI images, which consist of spatial registration, phase correction, re-gridding reconstruction, off-resonance effects reduction, density compensation, and Fourier transformation. Only the data in one diffusion direction were demonstrated for simplification.

be associated with two different bins when it fell into the overlapping interval, therefore increasing the number of blades sorted into each bin. Second, for each slice location of the binned data, an initial blade was selected to start searching the adjacent blade in either a clockwise or counter-clockwise direction. Two criteria were used to maximize the k-space uniformity by selecting the optimal combination of blades for PROPELLER-EPI reconstruction (Figure 3B): (1) the target desired N_B was determined for a 180° circular k-space coverage with specified blade size; and (2) the angular differences between any pair of two adjacent blades were as close as possible to the desired rotation angle (i.e., $180°/N_B$) with a pre-defined tolerance for the angular difference (e.g., +/−10% of the desired rotation angle). The blade selection process stopped when reaching the target N_B or no available blades fulfilling the second criterion. Then, for the rest of the blades without being selected, one of them was selected as an initial blade for starting another searching cycle with all blades in the same bin. The blade selection process was repeated until all blades in the same bin were selected for at least one combination. Finally, the N_B and K_{unif} were respectively recorded and calculated (Figure 3C), and the combination of blades with the highest N_B and K_{unif} was selected to produce the image for the corresponding bin by using conventional PROPELLER-EPI reconstruction[41] (Figure 3D). For all simulated and acquired data, only the reconstruction of six bins was performed for a fair comparison with the 4D-DW-ss-EPI technique which was originally demonstrated with six bins.

2.5 | Simulation experiments

A 4D Digital Extended Cardiac-Torso (XCAT) phantom[42] was used to evaluate the performance of 4D-DW-PROPELLER-EPI associated with N_r and F_s (i.e., 1/TR). For performing statistical analysis, each simulation was repeatedly performed 100 times with random variations of the respiratory period (3.33–5 s)[43] and chest motion (±5.5–7.1 mm along anteroposterior direction).[44]

2.5.1 | Generation of simulated 4D dataset

The simulation parameters for the XCAT phantom, coil sensitivity map, PROPELLER-EPI blade, and data binning were summarized in Supplementary Table S1. First, a total of 1360 individual 4D datasets with 200 dynamics in one respiratory cycle were generated with different combinations of 68 varying respiratory periods and 20 varying maximum chest wall motions. Afterwards, all 4D datasets were randomly concatenated to produce a single 4D dataset with varying respiratory cycles, and the corresponding synchronized respiratory signals were also produced accordingly. Then, a set of simulated eight-channel coil sensitivity maps with varying SNR in each channel was used for producing a multi-coil 4D dataset.

2.5.2 | Simulation of data sampling with different N_r and F_s

Different N_r and F_s were tested for investigating the performance of 4D-DW-PROPELLER-EPI. By considering (1) at least 20 acquisition repetitions needed for six bins in 4D-MRI[40] and (2) 12 blades needed for the 180° k-space coverage, the required N_r was estimated to be 240 (20×12) for sufficient data sampling at eight different F_s (i.e., TR = 1500, 2000, 2500, 3000, 3500, 4000, 4500, and 5000 ms). For each F_s, the 3D volume data were picked from the simulated multi-coil 4D dataset accordingly, and then sampled in k-space with PROPELLER-EPI blades using golden-angle rotation (i.e., the total number of blades = N_r). In addition, the T_2^* relaxation time of 20 ms[45] was applied to simulate the T_2^* signal decay effect along phase encoding during EPI readout with an ESP of 0.8 ms. Finally, all 3D volumetric blades were used to form a simulated raw dataset acquired at a specified F_s for the proposed 4D-DW-PROPELLER-EPI. In addition, to compare the performances between linear-angle and golden-angle multi-blade acquisitions for 4D-DW-PROPELLER-EPI, another simulated multi-blade dataset with 15-degree rotation at F_s of 1/(2000 ms) (i.e., TR = 2000 ms) was generated with other parameters identical to the simulation for golden-angle multi-blade acquisition.

2.5.3 | Simulation of data binning and reconstruction

All blades of each simulated raw dataset with golden-angle rotation were sorted using either conventional amplitude binning or *K*-B amplitude binning to generate the motion-resolved 4D-DW-PROPELLER-EPI data with six bins for each slice location (Supplementary Table S1). For the proposed *K*-B amplitude binning, the desired N_B was 18 for a 180° circular k-space coverage and the pre-defined angular difference between any two adjacent blades was 10°. For both conventional and *K*-B amplitude binning methods, the blades of each bin for each slice location were reconstructed with conventional PROPELLER-EPI reconstruction to produce two sets of final 4D motion-resolved images with six bins. The simulated multi-blades generated with 15-degree rotation were sorted into six bins by using *K*-B amplitude binning only, and then reconstructed to the six-bin 4D images with the same procedure.

2.5.4 | Data analysis of simulation experiments

All the analyses were performed by using MATLAB (version R2021a). To evaluate the effect of N_r and F_s on the data adequacy (i.e., image quality) of 4D-DW-PROPELLER-EPI for two different binning methods, 4D *Cpb* and 4D *Cpk* were calculated for each F_s at 12 different numbers of N_r (i.e., varying from 20 to 240 with an increment of 20) with the desired N_B of 18 and K_{unif} of 0.8 (i.e., > 80% K_{unif} for 180° k-space coverage). In addition, the medians of 4D *Cpb* and 4D *Cpk* at each N_r were measured from 100 repeated simulations to plot the completeness curves (i.e., ranging from 0 to 100%). The data adequacy was qualified when 4D *Cpb* and 4D *Cpk* achieved 95%, and the minimal requirement for N_r (defined as $N_{r,min}$) could also be determined. The structural similarity index measure (SSIM) was used to quantitatively compare the 4D images reconstructed with two different binning methods. Pearson correlation test was used to test the consistency of the tendency for completeness. Two-sample paired t-test was used to test the significant differences between the completeness curves. Furthermore, to compare the effect of different rotation angles on the data adequacy of 4D-DW-PROPELLER-EPI, similar data analysis (i.e., calculations of 4D *Cpb, 4D Cpk*, and SSIM) was also performed on the 100 repeated

simulations of linear-angle multi-blade acquisition (i.e., 15-degree rotation) at F_s of 1/(2000 ms).

2.6 | In vivo experiments

2.6.1 | Data acquisition

This study was approved by the local Institutional Review Board. Two sets of abdominal 4D-DWI data were acquired from two healthy volunteers with *b*-values of 0 s/mm^2 and 500 s/mm^2 at three orthogonal diffusion directions using a 1.5T MRI scanner (HDxt, GE Healthcare, Waukesha, WI) and a 12-channel phase-array body coil. First, The originally proposed 4D-DW-ss-EPI data were acquired with the scan parameters as follows: TR = 6700 ms, TE = 61.2 ms, FOV = 380 × 380 mm^2, matrix size = 128 × 128, slice thickness = 8.00 mm, number of slices = 20, number of repeated acquisition (N_r) = 20 for each diffusion direction, total acquisition time = 480 s. Second, the proposed 4D-DW-PROPELLER-EPI data with two different TRs was acquired with the scan parameters as follows: TR = 2000/3000 ms, TE = 60 ms, FOV = 380 × 380 mm^2, blade size = 128 × 32, rotation angle = 111.25°, slice thickness = 8.00 mm, number of slices = 14/20, number of multi-blades (N_r) = 90 for each diffusion direction, total acquisition time = 720/1080 s. During the acquisition of both datasets, a respiratory belt transducer with a sampling rate of 25 Hz was wrapped around the volunteer's upper abdomen to simultaneously record the respiratory signal. In addition, for the comparison of geometric fidelity, the 20s-breath-held T_2-weighted fast spin-echo (T_{2W}-FSE) images were acquired with TR/TE of 2250/85 ms, matrix size of 256 × 256, echo-train length = 16, and other geometric parameters identical to 4D-DWI acquisitions.

2.6.2 | Data binning and reconstruction

For 4D-DW-ss-EPI, images acquired for each diffusion direction at each slice location were sorted into six bins using conventional amplitude binning, and the images of each bin for each slice location were averaged to generate 4D-DWI images. For 4D-DW-PROPELLER-EPI, the multi-blade data acquired for each diffusion direction at each slice location were sorted into six bins using either conventional amplitude binning or *K*-B amplitude binning (with desired N_B = 18 for 180° circular k-space coverage). Subsequently, the sorted blades of each bin for each slice location were reconstructed with conventional PROPELLER-EPI reconstruction to generate the motion-resolved 4D-DWI image with six bins. Before data binning, the amplitudes of respiratory signals were normalized to a range between 0 and 1 corresponding to the largest chest wall motions during expiration and inspiration. Thus, six amplitude intervals were set without overlapping as 0 to 0.22, 0.22 to 0.39, 0.39 to 0.61, 0.61 to 0.72, 0.72 to 0.83, and 0.83 to 1 for conventional amplitude binning, and with overlapping as 0 to 0.28, 0.17 to 0.39, 0.33 to 0.61, 0.44 to 0.72, 0.67 to 0.83, and 0.78 to 1 for *K*-B amplitude binning.

2.6.3 | Data analysis

All the analyses were performed by using MATLAB (version R2021a). Motion-resolved 4D-DWI images produced from either 4D-DW-ss-EPI or 4D-DW-PROPELLER-EPI were compared by visual assessment and SSIM evaluation. In addition, 4D C*pb* and 4D C*pk* were calculated with the desired N_B and K_{unif} for evaluating the performance of 4D-DW-PROPELLER-EPI.

3 | RESULTS

3.1 | Simulation experiments

Figure 4 shows the completeness curves of 4D *Cpb* and 4D *Cpk* measured from the 100 repeatedly simulated data using either *K*-B amplitude binning (first rows of Figure 4A,B) or conventional amplitude binning (second rows of Figure 4A,B) under three different F_s (TRs of 2000, 3000, and 4000 ms). All the completeness curves under eight different F_s (TRs ranging from 2000 to 5000 ms) were shown in Supplementary Figures S1 and S2. It demonstrates that the completeness of 4D *Cpb* and 4D *Cpk* depends on N_r in a sigmoidal pattern for both *K*-B amplitude binning and conventional amplitude binning. For *K*-B amplitude binning with the data sampled under different F_s, all the 4D *Cpb* and 4D *Cpk* could achieve 95% completeness from $N_r \geq 90$ (first rows of Figure 4A,B). However, the conventional amplitude binning required N_r of 240 for achieving 95% completeness for both 4D *Cpb* and 4D *Cpk* (second rows of Figure 4A,B), suggesting that the proposed *K*-B amplitude binning can improve the acquisition efficiency for 4D-DW-PROPELLER-EPI with $N_{r,min}$ of 90 (i.e., total number of multi-blades = 90 for each diffusion direction). Pearson correlation analysis shows the completeness curves of 4D *Cpb* and 4D *Cpk* at different F_s were strongly correlated to each other for the two different binning methods ($p < 0.001$, all).

Furthermore, the two-sample paired t-test demonstrates no significant differences between 4D *Cpb* curves at different F_s ($0.062 < p < 0.065$, all) for *K*-B amplitude binning ($59.75 < M < 65.53$, $40.82 < SD < 44.22$)

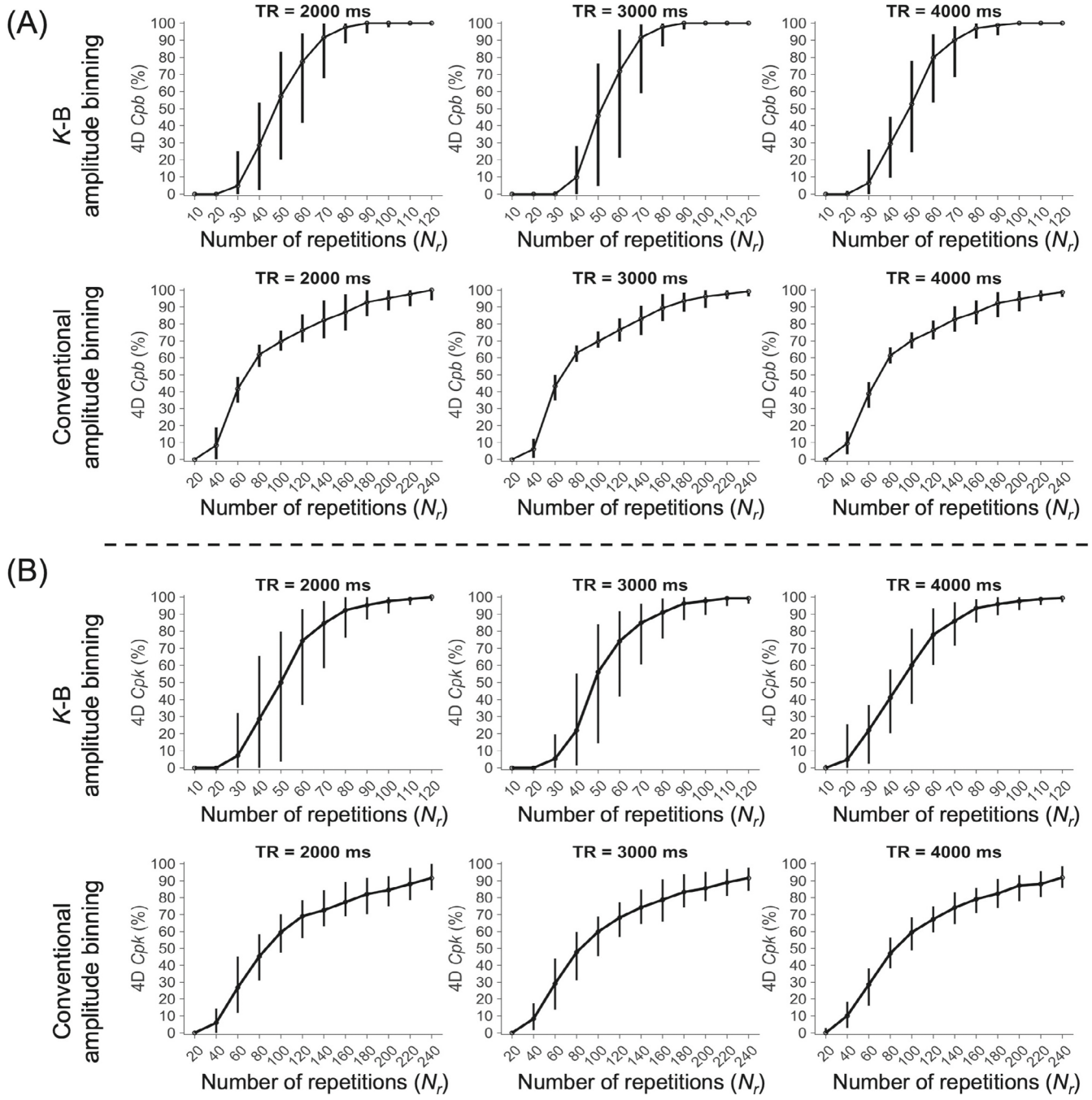

FIGURE 4 Simulation result of (A) 4D *Cpb* curves and (B) 4D *Cpk* curves measured from 100 repeatedly simulated 4D-DW-PROPELLER-EPI data using either *K*-B or conventional amplitude binning at varying F_s. It demonstrates that the completeness of 4D *Cpb* depends on N_r in a sigmoidal pattern for both *K*-B amplitude binning and conventional amplitude binning. All the 4D *Cpb* and 4D C*pk* curves could achieve 95% from N_r of 90 for *K*-B amplitude binning, whereas from N_r of more than 240 for conventional amplitude binning. This simulation result suggests that the acquisition efficiency could be substantially improved by using *K*-B amplitude binning for the proposed 4D-DW-PROPELLER-EPI (90 vs 240 for the total number of multi-blades needed for the reconstruction of six bins).

and conventional amplitude binning ($67.01 < M < 68.12$, $33.30 < SD < 34.75$). Similarly, no significant differences between 4D *Cpk* curves at different F_s ($0.058 < p < 0.072$, all) for *K*-B amplitude binning ($58.94 < M < 67.29$, $34.55 < SD < 41.76$) and conventional amplitude binning ($57.38 < M < 66.56$, $30.96 < SD < 32.48$).

Figure 5 shows the simulation result of the six-bin 4D-DWI images reconstructed from 4D-DW-PROPELLER-EPI ($N_r = 240$ and $F_s = 1/2000$ ms) using *K*-B amplitude binning and conventional amplitude binning, respectively. Compared with the ground truth data (i.e., first row of Figure 5), the images resulting from

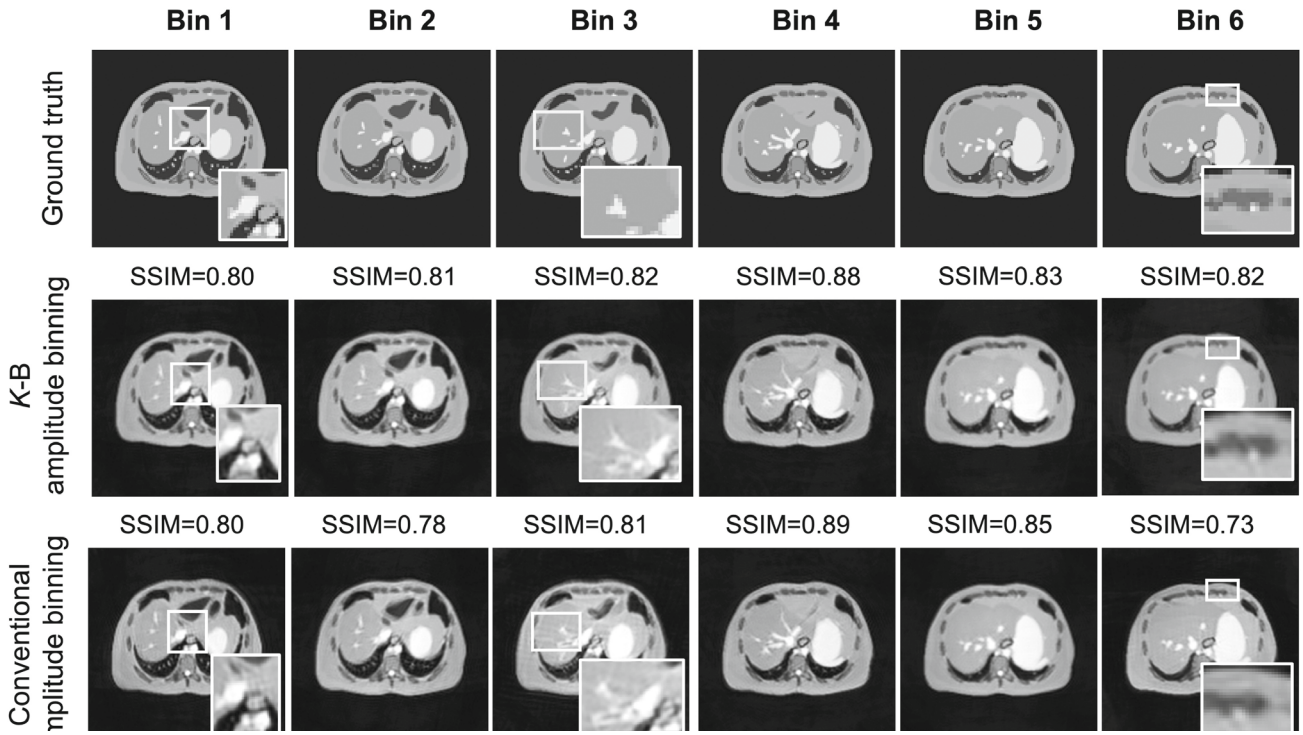

FIGURE 5 Simulation result of the six-bin 4D-DWI images reconstructed from 4D-DW-PROPELLER-EPI (simulated data acquisition with $N_r = 240$ and $F_s = 1/2000$ ms) using either *K*-B amplitude binning (second row) or conventional amplitude binning (third row), with the comparison to ground truth images generated from XCAT digital phantom (first row). The zoomed regions demonstrate that the images resulting from *K*-B amplitude binning show less streaking and blurring artifacts than those from conventional amplitude binning. Note that the blurring of reconstruction images was caused by the simulation of T_2^* windowing effect existing in the data acquisition of each blade.

K-B amplitude binning show less streaking and blurring artifacts than those from conventional amplitude binning (i.e., the zoomed regions in Figure 5). Also, the images resulting from *K*-B amplitude binning show slightly higher similarities and lower variations of similarities to the gold standard (SSIM: 0.83 ± 0.363) than those from conventional amplitude binning (SSIM: 0.82 ± 0.456). Note that the blurring of reconstructed images was caused by the simulation of T_2^* decay windowing effect existing in the data acquisition of each blade.

Figure 6 shows the simulation result for comparing the performance of 4D-DW-PROPELLER-EPI at F_s of 1/(2000 ms) between the uses of golden-angle rotation and 15-degree rotation. Figure 6A shows the 4D *Cpb* curves and the 4D *Cpk* values measured from the 100 repeatedly simulated multi-blade data with either golden-angle rotation or 15-degree rotation at N_r of 90. It demonstrates that the 4D *Cpb* could achieve 95% completeness from $N_r \geq 90$ for both golden-angle and linear-angle rotations. However, the 4D *Cpk* value for the multi-blade data with 15-degree rotation was significantly lower than that with golden-angle rotation ($p < 0.05$), suggesting that the acquisition of multi-blades with linear-angle rotation may lead to poor k-space sampling uniformity after the data binning for 4D-DW-PROPELLER-EPI. Figure 6B shows that the six-bin 4D-DWI images reconstructed from the multi-blades with the 15-degree rotation had more blurring and streaking artifacts than those with the golden-angle rotation (pointed by the yellow arrows in Figure 6).

3.2 | In vivo experiments

Figure 7 compares the images reconstructed from T_{2W}-FSE, 4D-DW-PROPELLER-EPI with *K*-B amplitude binning (at TR of 2000 ms), and originally proposed 4D-DW-ss-EPI. A contour of the liver was drawn on T_{2W}-FSE and then pasted on the other two images for assessing the geometric fidelity. Results show that 4D-DW-PROPELLER-EPI with *K*-B amplitude binning can achieve superior geometric fidelity over 4D-DW-ss-EPI, which has prominent geometric distortion (arrows in the right panel of Figure 7).

Figure 8 shows the in vivo results of two sets of six-bin 4D-DWI images produced from the proposed 4D-DW-PROPELLER-EPI ($N_r = 90$ for each diffusion direction) with *K*-B amplitude binning at TR of 2000 ms

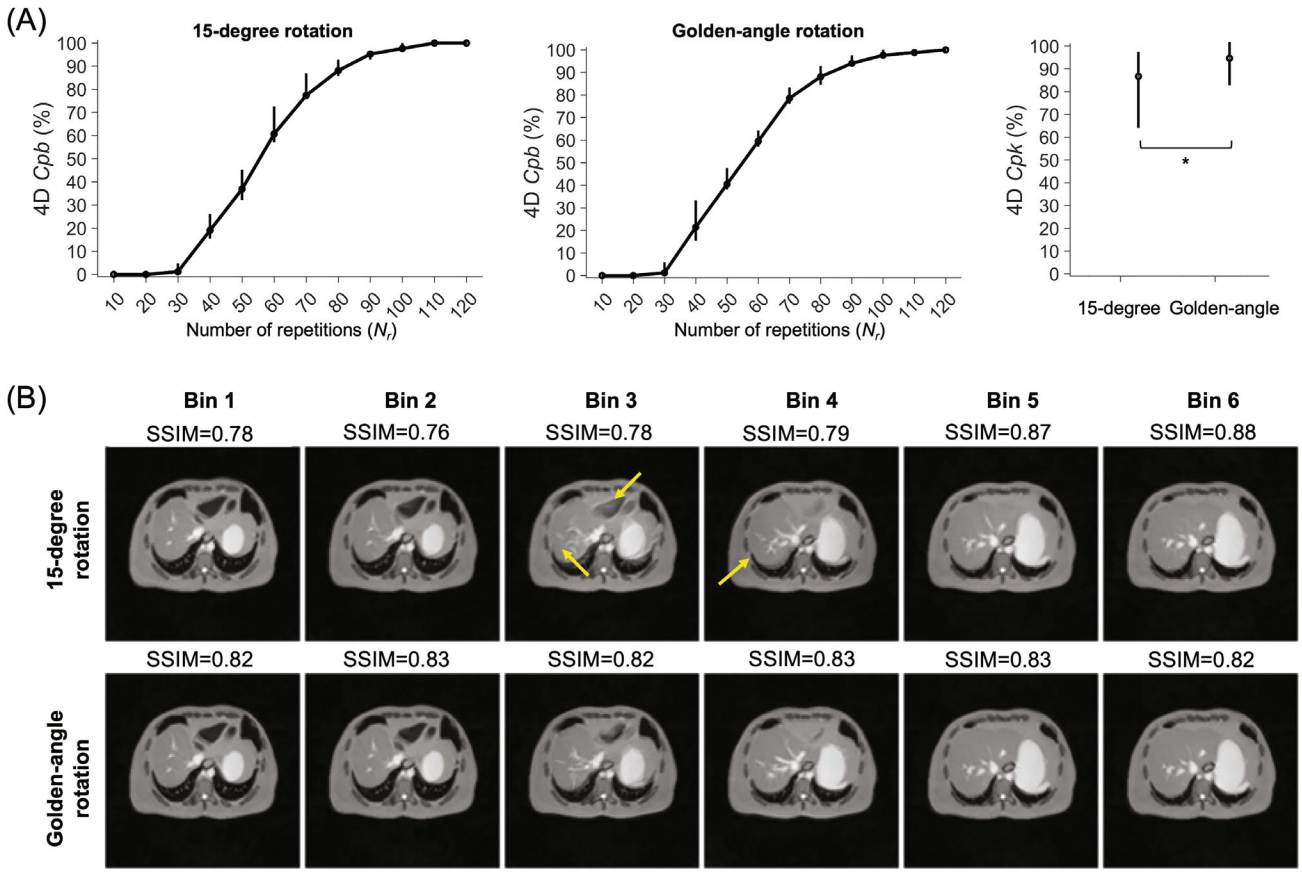

FIGURE 6 Simulation result for comparing the performance of 4D-DW-PROPELLER-EPI at F_s of 1/(2000 ms) between the uses of golden-angle rotation and 15-degree rotation. (A) Completeness curves of 4D *Cpb* and values of 4D *Cpk* measured from the 100 repeatedly simulated multi-blade data with either golden-angle rotation or 15-degree rotation at N_r of 90. The 4D *Cpb* could achieve 95% completeness from $N_r \geq 90$ for both golden-angle and linear-angle rotations. (B) The six-bin 4D-DWI images reconstructed from multi-blades with the 15-degree rotation show more blurring and streaking artifacts than those with the golden-angle rotation angle (pointed by yellow arrows).

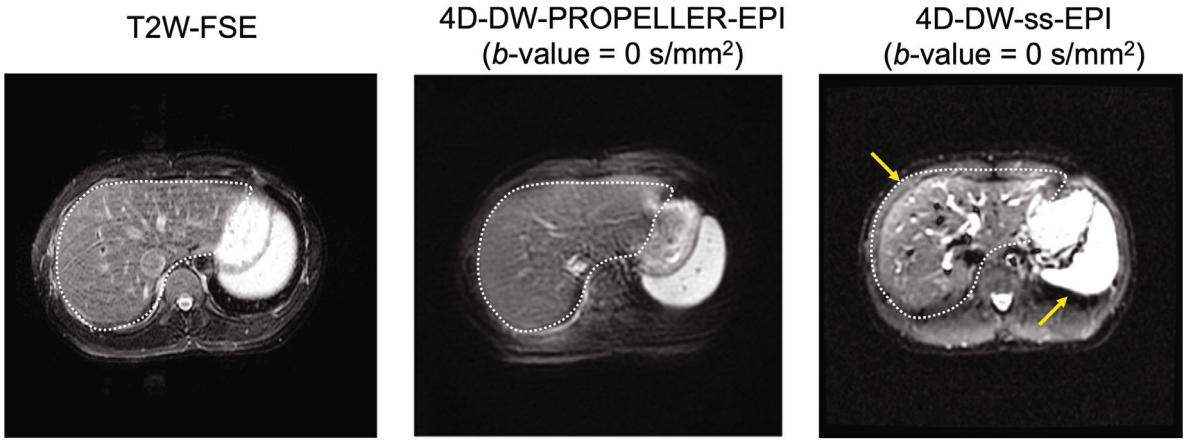

FIGURE 7 Comparison of in vivo abdominal images reconstructed from T_{2W}-FSE, 4D-DW-PROPELLER-EPI with *K*-B amplitude binning, and 4D-DW-ss-EPI. By observing the liver contour drawn on T_{2W}-FSE image, it shows that 4D-DW-PROPELLER-EPI can produce distortion-free 4D-DWI images. Yellow arrows in the right picture point to the geometric distortions present in the liver and spleen for the 4D-DWI images produced from 4D-DW-ss-EPI.

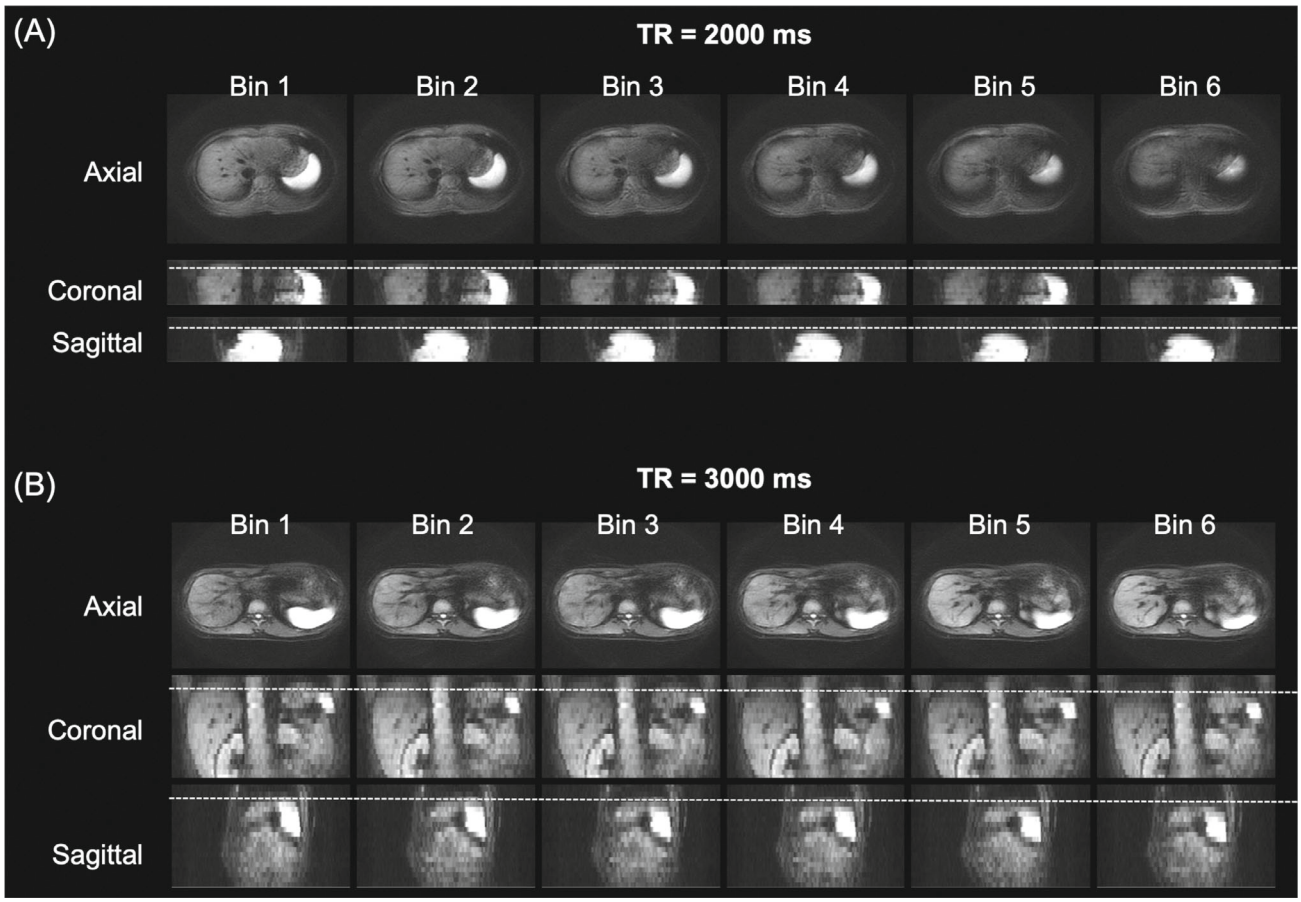

FIGURE 8 The in vivo results of two sets of the six-bin 4D-DWI images produced from proposed 4D-DW-PROPELLER-EPI ($N_r = 90$ for each diffusion direction) with *K*-B amplitude binning at TR of (A) 2000 ms and (B) 3000 ms for two different subjects, and the corresponding reformatted 4D-DWI images in coronal and sagittal planes. Although both F_s could achieve high-quality 4D-DWI images, the higher F_s (i.e., shorter TR) led to more limited volume coverage along slice direction.

(Figure 8A) and 3000 ms (Figure 8B) for two different subjects, and the corresponding reformatted 4D-DWI images in coronal and sagittal planes. Although both F_s could achieve high-quality 4D-DWI images, the higher F_s (i.e., shorter TR) led to more limited volume coverage along slice direction.

Figure 9 compares the representative 4D-DWI images produced by 4D-DW-ss-EPI and 4D-DW-PROPELLER-EPI at TR of 2000 ms (Figure 9A) and 3000 ms (Figure 9B). Either conventional amplitude binning or *K*-B amplitude binning was used to sort the multi-blade data of 4D-DW-PROPELLER-EPI, and all the 4D-DWI images produced by 4D-DW-PROPELLER-EPI (second and third rows of Figure 9A,B) show superior geometric fidelity and image quality to 4D-DW-ss-EPI (first rows of Figure 9A,B). In addition, the 4D-DWI images produced by 4D-DW-PROPELLER-EPI with *K*-B amplitude binning (second rows of Figure 9A,B; zoomed regions) had less streaking artifacts than those with conventional amplitude binning (third rows of Figure 9A,B; zoomed regions), suggesting that *K*-B amplitude binning can achieve marginal to moderate improvement on the performance of 4D-DW-PROPELLER-EPI. The reconstruction of a whole set of 4D-DW-PROPELLER-EPI data required 27.6 min for a slice location of 14 and 39.5 min for a slice location of 20, using a PC equipped with 64-bit Windows 11, a 3.20 GHz Intel Core i9-12900KF processor, and 4 GB of memory.

Figure 10 shows the resulted N_B and measured K_{unif} after the binning of multi-blades acquired with 4D-DW-PROPELLER-EPI (at TR of 2000 ms) using either *K*-B amplitude binning or conventional amplitude binning. Different colored boxplots represent different diffusion directions, and each boxplot shows the resulted N_B and measured K_{unif} from all slice locations in the same bin. A total of 96.4% of the N_B resulting from *K*-B amplitude binning was equal to 18, whereas those from conventional amplitude binning were distributed from 4 to 30. In addition, 95.2% of the measured K_{unif} were greater than 0.8 for *K*-B amplitude binning, whereas those from conventional amplitude binning were from 0.61 to 0.84. Therefore, the 4D *Cpb* of *K*-B amplitude binning and conventional

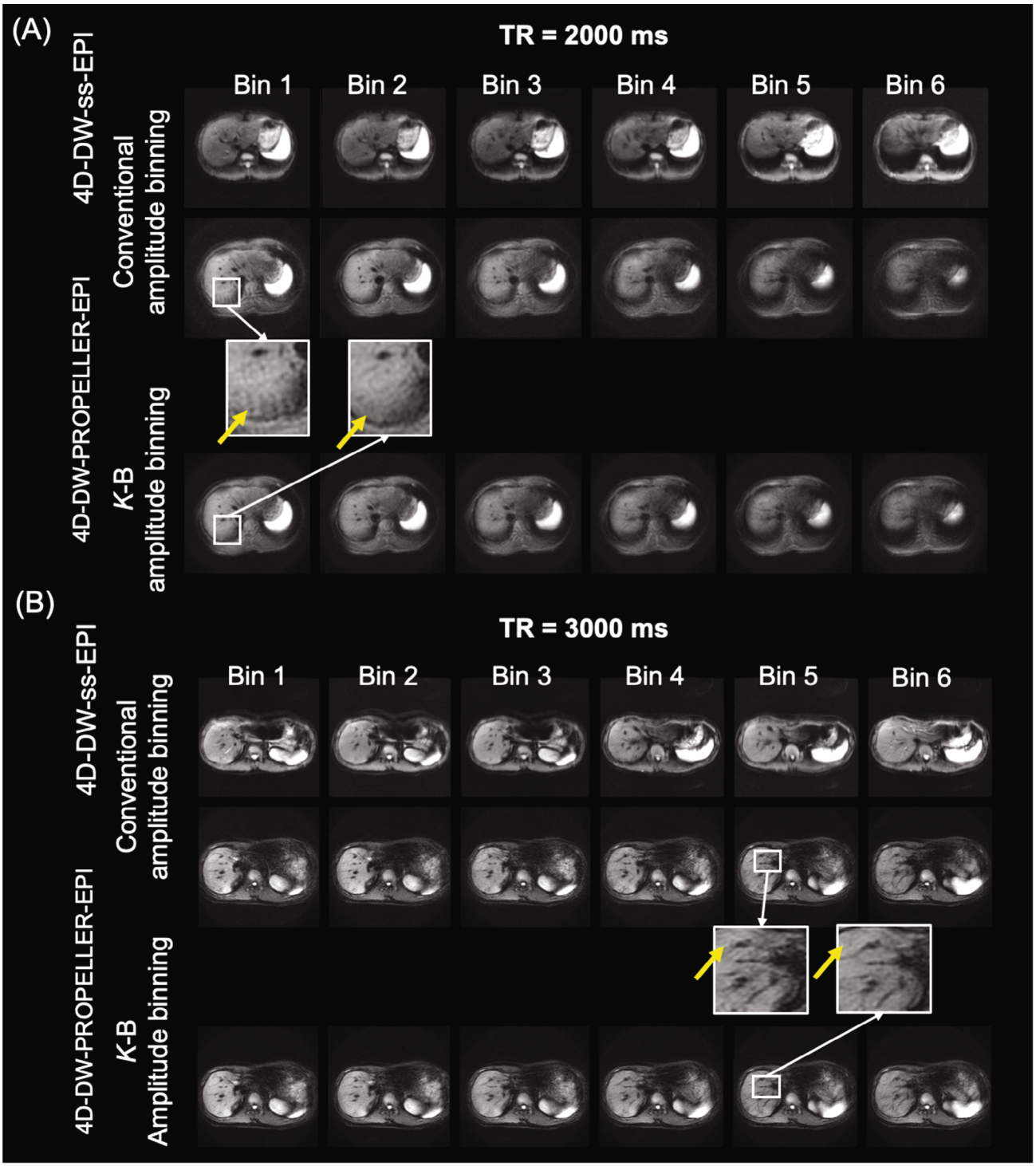

FIGURE 9 In vivo result of the representative axial six-bin 4D-DWI images produced by 4D-DW-ss-EPI with conventional amplitude binning (first row), and 4D-DW-PROPELLER-EPI with either conventional amplitude binning (second row) or *K*-B amplitude binning (third row) at TR of (A) 2000 ms and (B) 3000 ms. All the 4D-DWI images produced by 4D-DW-PROPELLER-EPI show superior geometric fidelity and image quality to 4D-DW-ss-EPI. The 4D-DWI images produced by 4D-DW-PROPELLER-EPI with *K*-B amplitude binning (second rows of A and B; zoomed regions) had less streaking artifacts than those with conventional amplitude binning (third rows of A and B; zoomed regions), suggesting that *K*-B amplitude binning can achieve marginal to moderate improvement on the performance of 4D-DW-PROPELLER-EPI. The reconstruction of a whole set of 4D-DW-PROPELLER-EPI data required 27.6 min for a slice location of 14 and 39.5 min for a slice location of 20, using a PC equipped with 64-bit Windows 11, a 3.20 GHz Intel Core i9-12900KF processor, and 4 GB of memory.

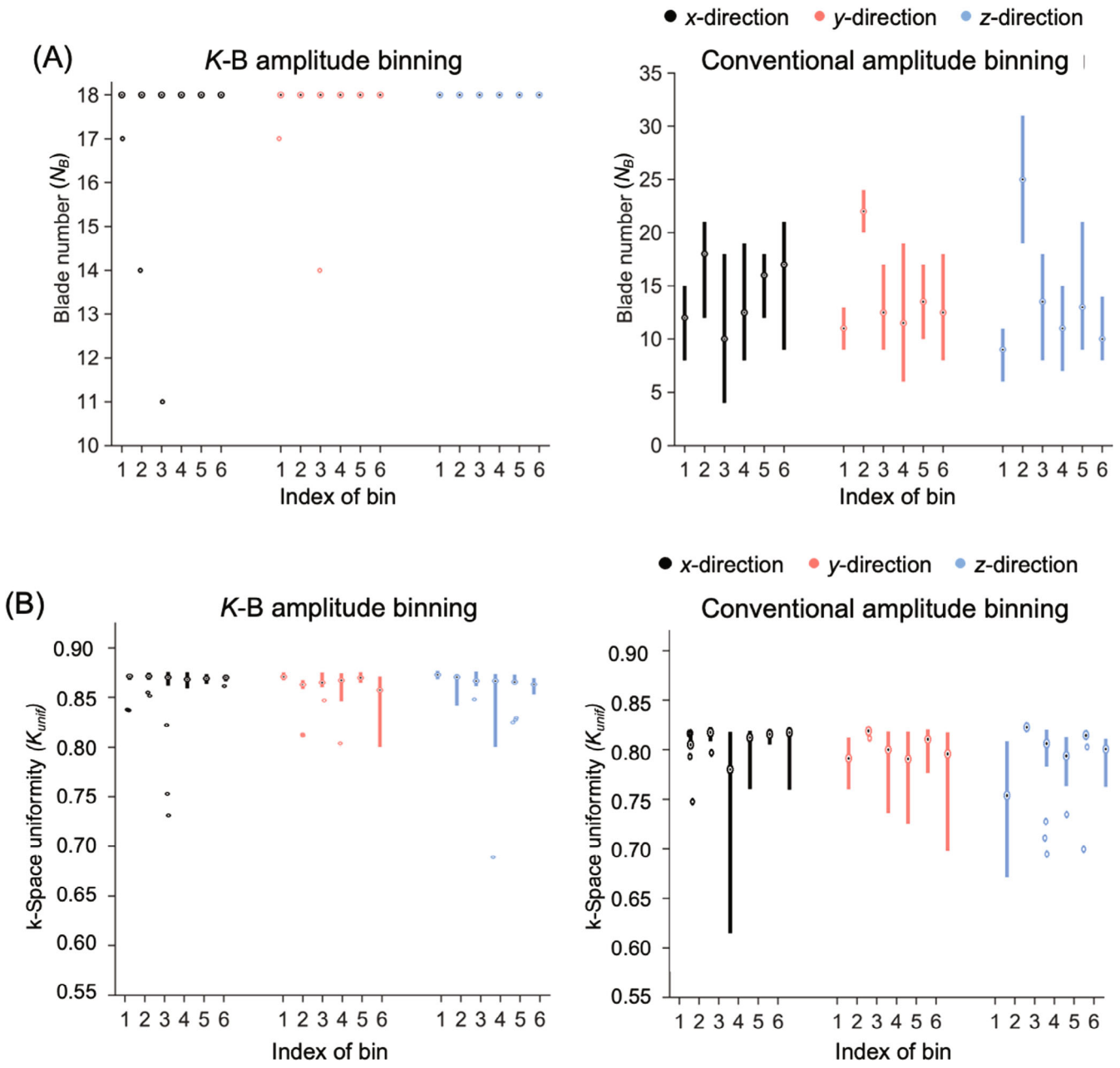

FIGURE 10 In vivo results of (A) N_B and (B) K_{unif} measured after the binning of multi-blades acquired with proposed 4D-DW-PROPELLER-EPI using either *K*-B amplitude binning (left column) or conventional amplitude binning (right column) at TR of 2000 ms. Different colored boxplots represent different diffusion directions, and each boxplot shows the resulted N_B and measured K_{unif} from all slice locations in the same bin. (A) A total of 96.4% of the N_B resulting from *K*-B amplitude binning was equal to 18, whereas those from conventional amplitude binning were distributed from 4 to 30. (B) A total of 95.2% of the measured K_{unif} were greater than 0.8 for *K*-B amplitude binning, whereas those for conventional amplitude binning were from 0.61 to 0.84. Those results suggest that the *K*-B amplitude binning method is advantageous to the data reconstruction using PROPELLER-EPI for the proposed 4D-DW-PROPELLER-EPI.

amplitude binning were 96.4% and 54.3%, and the 4D *Cpk* of *K*-B amplitude binning and conventional amplitude binning were 95.2% and 57.4%, respectively. Similar results were also observed from the binned data acquired with 4D-DW-PROPELLER-EPI at TR of 3000 ms (Supplementary Figure S3).

4 | DISCUSSION AND CONCLUSIONS

For the IGRT, 4D-DW-ss-EPI has recently been proposed to provide superior tumor-to-tissue contrast compared to conventional 4D-MRI, thereby improving the treatment

planning.[7] However, the routinely used DW-ss-EPI technique can only provide limited image quality and low geometric fidelity in imaging the abdomen. Because IGRT treatment planning highly depends on the accurate estimations of turmor volume and its location in relation to other organs, the presence of geometric distortion in 4D-DW-ss-EPI may affect the accuracy of dose calculation for the target volume and organs at risk.[7] In this study, the 4D-DW-PROPELLER-EPI was proposed to enable motion-resolved abdominal 4D-DWI with better geometric fidelity compared with 4D-DW-ss-EPI (Figures 7 and 9).

The DW-PROPELLER-EPI was originally developed for achieving distortion-free high-resolution brain DWI,[41] and also preliminarily tested for its feasibility in free-breathing liver DWI with motion-compensation. To enable motion-resolved abdominal 4D-DWI using DW-PROPELLER-EPI with motion-compensation for the reconstructed images of each bin, first, the golden-angle rotation for multi-blade acquisition was adopted to better introduce temporal incoherency between the sampling of blades and respiratory cycles. The proposed 4D-DW-PROPELLER-EPI with golden-angle rotation can improve the distribution of k-space blades associated with different respiratory phases (i.e., respiratory bin), as well as reduce the possible redundancy of k-space blades caused by the use of linear-angle rotation (as the lower k-space uniformity demonstrated in Figure 6 for the 15-degree multi-blade acquisition). Second, the long-axis multi-blade acquisition was used to shorten the ETL (i.e., less phase-encoding for the blade of long-axis PROPELLER-EPI), thereby improving the sampling rate F_s (i.e., the frame rate of repeated acquisition) compared with 4D-DW-ss-EPI for same slice coverage (i.e., TRs of 3000 ms vs. 6700 ms). For a desired number of bins, the improved F_s can ensure that the multi-blade data relatively equally fall into each bin after data sorting according to the surrogate respiratory signal.[40,46] Third, the *K*-B amplitude binning was developed to sort the multi-blades into different bins that can optimize the subsequent image reconstruction using conventional PROPELLER-EPI reconstruction.

The use of *K*-B amplitude binning can search for the best combination of blades from the same bin by simultaneously considering the number of blades (N_B) and the uniformity of k-space. Thus, the selection of blades from the same bin can fulfill the requirement of subsequent conventional PROPELLER-EPI reconstruction as much as possible. In other words, sufficient N_B and high K_{unif} of the selected blades are necessary to produce high-quality images for each bin at each slice location. In addition, the variations in amplitude and period of the surrogate respiratory signal may reduce the adequacy of blades in each bin for the data sorting, and therefore the overlapping between amplitude binning intervals was used to increase the number of blades falling into each desired bin. Although including more blades into one amplitude bin may give rise to data inconsistency associated with varying respiration, nevertheless, the intrinsic capacity of motion reduction in PROPELLER-EPI reconstruction can alleviate this problem.[31]

The simulation experiment with a digital XCAT phantom was conducted to evaluate the feasibility and performance of 4D-DW-PROPELLER-EPI with different acquisition parameters (e.g., N_r and F_s). Also, the practical respiratory condition was mimicked during the simulation, such as the presence of varying respiratory periods and chest wall motion during the data sampling. Simulation results of 4D *Cpb* and 4D *Cpk* show that the dependency of data adequacy on N_r (i.e., number of multi-blades for each diffusion direction) is in agreement with previous 4D-MRI studies[40] (Figure 4). To ensure sufficient data for producing images with satisfactory quality, 4D *Cpb* and 4D *Cpk* are required to be equal to or over 95%. As shown in Figure 4, at a desired N_B (i.e., 18 blades), the $N_{r,min}$ of 4D-DW-PROPELLER-EPI with *K*-B amplitude binning is significantly lower than that with conventional binning ($N_{r,min} = 90$ vs. 240), suggesting that *K*-B amplitude binning can also improve the acquisition efficiency for 4D-DW-PROPELLER-EPI. Therefore, N_r of 90 was set for the in vivo experiments in order to acquire the data from healthy subjects at a reasonable time. In addition, compared with conventional amplitude binning, *K*-B amplitude binning can produce simulated and in vivo 4D-DWI images with less blurring and streaking artifacts (Figures 5 and 9), owing to the better K_{unif} for binned data (Figure 10B). Furthermore, the TRs of 2000 and 3000 ms were tested for the proposed 4D-DW-PROPELLER-EPI with a fixed N_r of 90 (for each diffusion direction), verifying that the *K*-B amplitube binning can improve the robustness in high-quality 4D-DW-PROPELLER-EPI (Figures 8 and 9). In contrast, the use of conventional amplitude binning for 4D-DW-PROPELLER-EPI can lead to varying image quality, due to the variations of N_B and relatively low K_{unif} across different bins (Figure 10A).

Although only the reconstruction of six bins for the proposed 4D-DW-PROPELLER-EPI with *K*-B amplitude binning was demonstrated, any other number of reconstructed bins can also be chosen from the typically desired range for the 4D-MRI applications (i.e., 4–10 bins[3]). To optimize the image reconstruction according to the desired number of bins and the overlapping between amplitude intervals, another simulation experiment is required to estimate the $N_{r,min}$ (i.e., the minimal requirement for the total number of multi-blades) by evaluating the 4D *Cpb* and 4D *Cpk* (i.e., both need to be >95%). Taking

10 bins with 15% overlapping between amplitude intervals as an example, the corresponding simulation result shows that an $N_{r,min}$ of 220 is required, therefore increasing the total acquisition time compared with the reconstruction of six bins (first column of Supplementary Figures S4A and S4B). In addition, the overlapping between amplitude intervals can be enlarged to reduce the total number of multi-blades needed for the data binning (simulations with 25%, 35%, and 45% overlappings between the amplitude intervals are also shown in Supplementary Figure S4). However, the reconstructed images of each bin may suffer from imaging blurring because the extended amplitude interval can introduce prominent variations of respiratory motion among the blades sorted into the same bin. Further study is needed to investigate the effect of extended amplitude interval on reconstructed image quality for 4D-DW-PROPELLER-EPI with *K*-B amplitude binning.

There are several limitations to this study. First, although DW-PROPELLER-EPI can produce high-quality DWI images without geometric distortion, the different off-resonance effects in each blade can cause blurring in the final reconstructed images.[30] Particularly in abdominal imaging, performing proper shimming is often required to reduce the off-resonance effects. Also, incorporating off-resonance correction into the conventional PROPELLER-EPI reconstruction may help further improve the image quality of 4D-DW-PROPELLER-EPI.[30] Second, despite superior geometric fidelity compared with 4D-DW-ssEPI, similar to other multi-shot EPI techniques, the proposed 4D-DW-PROPELLER-EPI requires substantially increased acquisition time (ranging from 12 to 18 min for covering 14 to 20 slices), which can hinder its clinical adoption. Other alternative multi-shot PROPELLER techniques based on gradient and spin echo, such as X-PROP[47] and Steer-PROP,[48] can also achieve high-quality and high-fidelity DWI with more reasonable acquisition time. Therefore, they may also potentially enable high-quality abdominal 4D-DWI for IGRT application. Third, the quantitative measurement of ADC was not evaluated for the proposed 4D-DW-PROPELLER-EPI. Future investigation with a large cohort of healthy subjects may be required for assessing the robustness of 4D-DW-PROPELLER-EPI in ADC measurement.

In conclusion, the simulation and preliminary in vivo experiments demonstrate the feasibility of 4D-DW-PROPELLER-EPI for achieving high-quality 4D-DWI with high geometric fidelity, thereby potentially benefiting IGRT treatment planning.

ACKNOWLEDGMENTS

The work was supported by grants from Hong Kong Research Grant Council (GRF 17106820, GRF 17125321, and ECS 24213522).

ORCID

Lu Wang https://orcid.org/0000-0003-4698-1580
Hing-Chiu Chang https://orcid.org/0000-0001-8634-328X

REFERENCES

1. Kwong Y, Mel AO, Wheeler G, Troupis JM. F our-dimensional computed tomography (4DCT): a review of the current status and applications. *J Med Imaging Radiat Oncol*. 2015;59:545-554.
2. Lee KH, Lee S, Park JH, et al. Risk of hematologic malignant neoplasms from abdominopelvic computed tomographic radiation in patients who underwent appendectomy. *JAMA Surg*. 2021;156:343-351.
3. Stemkens B, Paulson ES, Tijssen RH. Nuts and bolts of 4D-MRI for radiotherapy. *Phys Med Biol*. 2018;63:21TR01.
4. Wang C, Yin FF. 4D-MRI in radiotherapy. *Magnetic Resonance Imaging*. IntechOpen; 2019.
5. Kele PG, van der Jagt EJ. Diffusion weighted imaging in the liver. *World J Gastroenterol: WJG*. 2010;16:1567-1576.
6. Naganawa S, Kawai H, Fukatsu H, et al. Diffusion-weighted imaging of the liver: technical challenges and prospects for the future. *Magn Reson Med Sci*. 2005;4:175-186.
7. Liu Y, Zhong X, Czito BG, et al. Four-dimensional diffusion-weighted MR imaging (4D-DWI): a feasibility study. *Med Phys*. 2017;44:397-406.
8. Zaitsev M, Maclaren J, Herbst M. Motion artifacts in MRI: a complex problem with many partial solutions. *J Magn Reson Imaging*. 2015;42:887-901.
9. Erasmus LJ, Hurter D, Naudé M, Kritzinger HG, Acho S. A short overview of MRI artefacts. *S Afr J Radiol*. 2004;8:13.
10. Morani AC, Elsayes KM, Liu PS, et al. Abdominal applications of diffusion-weighted magnetic resonance imaging: where do we stand. *World J Radiol*. 2013;5:68-80.
11. Chow LC, Bammer R, Moseley ME, Sommer FG. Single breath-hold diffusion-weighted imaging of the abdomen. *J Magn Reson Imaging*. 2003;18:377-382.
12. Taouli B, Koh DM. Diffusion-weighted MR imaging of the liver. *Radiology*. 2010;254:47-66.
13. Chen X, Qin L, Pan D, et al. Liver diffusion-weighted MR imaging: reproducibility comparison of ADC measurements obtained with multiple breath-hold, free-breathing, respiratory-triggered, and navigator-triggered techniques. *Radiology*. 2014;271:113-125.
14. Abdelnour AF, Nehmeh SA, Pan T, et al. Phase and amplitude binning for 4D-CT imaging. *Phys Med Biol*. 2007;52:3515-3529.
15. Bammer R, Keeling SL, Augustin M, et al. Improved diffusion-weighted single-shot echo-planar imaging (EPI) in stroke using sensitivity encoding (SENSE). *Magn Reson Med*. 2001;46:548-554.
16. Liu W, Xuna Z, Yajun M, Xin T, Jia-Hong G. DWI using navigated interleaved multishot EPI with realigned GRAPPA reconstruction. *Magn Reson Med*. 2016;75:280-286.
17. Hori M, Ichikawa T, Sou H, et al. Improving diffusion-weighted imaging of liver with SENSE technique: a preliminary study. *Nihon Igaku Hoshasen Gakkai Zasshi*. 2003;63:177-179.
18. Taouli B, Sandberg A, Stemmer A, et al. Diffusion-weighted imaging of the liver: comparison of navigator triggered and breathhold acquisitions. *J Magn Reson Imaging*. 2009;30:561-568.

19. Dai E, Zhang Z, Ma X, et al. The effects of navigator distortion and noise level on interleaved EPI DWI reconstruction: a comparison between image-and k-space-based method. *Magn Reson Med*. 2018;80:2024-2032.
20. An H, Ma X, Pan Z, Guo H, Lee EYP. Qualitative and quantitative comparison of image quality between single-shot echo-planar and interleaved multi-shot echo-planar diffusion-weighted imaging in female pelvis. *Eur Radiol*. 2020;30:1876-1884.
21. Holdsworth SJ, Skare S, Newbould RD, Guzmann R, Blevins NH, Bammer R. Readout-segmented EPI for rapid high resolution diffusion imaging at 3T. *Eur J Radiol*. 2008;65:36-46.
22. Heidemann RM, Porter DA, Anwander A, et al. Diffusion imaging in humans at 7T using readout-segmented EPI and GRAPPA. *Magn Reson Med*. 2010;64:9-14.
23. Peng S, Guo Y, Zhang X, et al. High-resolution DWI with simultaneous multi-slice readout-segmented Echo planar imaging for the evaluation of malignant and benign breast lesions. *Diagnostics*. 2021;11:2273.
24. Chang HC, Chen G, Chung HW, et al. Multi-shot diffusion-weighted MRI with multiplexed sensitivity encoding (MUSE) in the assessment of active inflammation in Crohn's disease. *J Magn Reson Imaging*. 2022;55:126-137.
25. Skare S, Newbould RD, Clayton DB, Bammer R. Propeller EPI in the other direction. *Magn Reson Med*. 2006;55:1298-1307.
26. Chou MC, Huang TY, Chung HW, Hsieh TJ, Chang HC, Chen CY. Q-ball imaging with PROPELLER EPI acquisition. *NMR Biomed*. 2013;26:1723-1732.
27. Holdsworth SJ, Yeom KW, Moseley ME, Skare S. Fast susceptibility-weighted imaging with three-dimensional short-axis propeller (SAP)-echo-planar imaging. *J Magn Reson Imaging*. 2015;41:1447-1453.
28. Krämer M, Jochimsen TH, Reichenbach JR. Functional magnetic resonance imaging using PROPELLER-EPI. *Magn Reson Med*. 2012;68:140-151.
29. Fair MJ, Wang F, Dong Z, Reese TG, Setsompop K. Propeller echo-planar time-resolved imaging with dynamic encoding (PEPTIDE). *Magn Reson Med*. 2020;83:2124-2137.
30. Wang L, Li T, Cai J, Chang HC. Motion-resolved four-dimensional abdominal diffusion-weighted imaging using propeller Echo-planar imaging (4D-DW-propeller-EPI). In *Proceedings of the 29th ISMRM & SMRT Annual Meeting & Exhibition*; 2021:#316.
31. Chang HC, Wang L, Chen G, et al. Repeatability of liver apparent diffusion coefficient measurement using free-breathing diffusion-weighted propeller Echo-planar imaging. In *Proceedings of the 29th ISMRM & SMRT Annual Meeting & Exhibition*; 2021:#318.
32. Wen Q, Feng L, Zhou K, Wu YC. Rapid golden-angle diffusion-weighted propeller MRI for simultaneous assessment of ADC and IVIM. *Neuroimage*. 2020;223:117327.
33. Feng L, Grimm R, Block KT, et al. Golden-angle radial sparse parallel MRI: combination of compressed sensing, parallel imaging, and golden-angle radial sampling for fast and flexible dynamic volumetric MRI. *Magn Reson Med*. 2014;72:707-717.
34. Feng L, Delacoste J, Smith D, et al. Simultaneous evaluation of lung anatomy and ventilation using 4D respiratory-motion-resolved ultrashort echo time sparse MRI. *J Magn Reson Imaging*. 2019;49:411-422.
35. Chandarana H, Feng L, Ream J, et al. Respiratory motion-resolved compressed sensing reconstruction of free-breathing radial acquisition for dynamic liver MRI. *Invest Radiol*. 2015;50:749-756.
36. Feng L, Axel L, Chandarana H, Block KT, Sodickson DK, Otazo R. XD-GRASP: golden-angle radial MRI with reconstruction of extra motion-state dimensions using compressed sensing. *Magn Reson Med*. 2016;75:775-788.
37. Chen N k, Wyrwicz AM. Removal of EPI Nyquist ghost artifacts with two-dimensional phase correction. *Magn Reson Med*. 2004;51:1247-1253.
38. Chen NK, Avram AV, Song AW. Two-dimensional phase cycled reconstruction for inherent correction of echo-planar imaging Nyquist artifacts. *Magn Reson Med*. 2011;66:1057-1066.
39. Chang HC, Chen NK, Chuang TC, Juan CJ, Wu ML, Chung HW. PROPELLER-EPI improved by 2D phase cycled reconstruction. In *Proceedings of the 20th ISMRM Annual Meeting*; 2012:#2447.
40. Liu Y, Yin FF, Czito BG, Bashir MR, Cai J. T_2-weighted four dimensional magnetic resonance imaging with result-driven phase sorting. *Med Phys*. 2015;42:4460-4471.
41. Wang FN, Huang TY, Lin FH, et al. PROPELLER EPI: an MRI technique suitable for diffusion tensor imaging at high field strength with reduced geometric distortions. *Magn Reson Med*. 2005;54:1232-1240.
42. Segars WP, Tsui BM, Cai J, Yin FF, Fung GS, Samei E. Application of the 4-D XCAT phantoms in biomedical imaging and beyond. *IEEE Trans Med Imaging*. 2017;37:680-692.
43. Ambekar MR, Prabhu S. A novel algorithm to obtain respiratory rate from the PPG signal. *Int J Comput Appl*. 2015;126:9-12.
44. Lowanichkiattikul C, Dhanachai M, Sitathanee C, Khachonkham S, Khaothong P. Impact of chest wall motion caused by respiration in adjuvant radiotherapy for postoperative breast cancer patients. *SpringerPlus*. 2016;5:1-8.
45. Labranche R, Gilbert G, Cerny M, et al. Liver iron quantification with MR imaging: a primer for radiologists. *Radiographics*. 2018;38:392-412.
46. Tryggestad E, Flammang A, Han-Oh S, et al. Respiration-based sorting of dynamic MRI to derive representative 4D-MRI for radiotherapy planning. *Med Phys*. 2013;40:051909.
47. Li Z, Pipe JG, Lee CY, Debbins JP, Karis JP, Huo D. X-PROP: a fast and robust diffusion-weighted propeller technique. *Magn Reson Med*. 2011;66:341-347.
48. Srinivasan G, Rangwala N, Zhou XJ. Steer-PROP: a GRASE-PROPELLER sequence with interecho steering gradient pulses. *Magn Reson Med*. 2018;79:2533-2541.

SUPPORTING INFORMATION

Additional supporting information may be found in the online version of the article at the publisher's website.

Table S1. The parameters of simulation experiments.

Figure S1. Simulation result of 4D *Cpb* curves measured from 100 repeatedly simulated 4D-DW-PROPELLER-EPI data for the reconstruction of six bins using either (A) *K*-B amplitude binning or (B) conventional amplitude binning at varying F_s.

Figure S2. Simulation result of 4D *Cpk* curves measured from 100 repeatedly simulated 4D-DW-PROPELLER-EPI

data for the reconstruction of six bins using either (A) *K*-B amplitude binning or (B) conventional amplitude binning at varying F_s.

Figure S3. In vivo results of (A) N_B and (B) K_{unif} measured after the binning of multi-blades acquired with proposed 4D-DW-PROPELLER-EPI using either *K*-B amplitude binning or conventional amplitude binning at TR of 3000 ms.

Figure S4. Simulation result of (A) 4D *Cpb* and (B) 4D *Cpk* curves measured from 100 repeatedly simulated 4D-DW-PROPELLER-EPI data for the reconstruction of 10 bins using *K*-B amplitude binning with 15%, 25%, 35%, and 45% overlapping between the amplitude intervals of two adjacent bins.

How to cite this article: Wang L, Li T, Cai J, Chang H-C. Motion-resolved four-dimensional abdominal diffusion-weighted imaging using PROPELLER EPI (4D-DW-PROPELLER-EPI). *Magn Reson Med*. 2023;90:2454-2471. doi: 10.1002/mrm.29802